Robotica (2018) volume 36, pp. 1757–1779. © Cambridge University Press 2018
doi:10.1017/S0263574718000723

Passive and active rehabilitation control of human upper-limb exoskeleton robot with dynamic uncertainties

Brahim Brahmi†*, Maarouf Saad†, Cristobal Ochoa Luna‡, Philippe S. Archambault‡, and Mohammad H. Rahman§

†*Electrical Engineering Department, École de technologie supérieure, Montreal, Canada. E-mail: maarouf.saad@etsmtl.ca*
‡*School of Physical & Occupational Therapy, McGill University; Centre for Interdisciplinary Research in Rehabilitation of Greater Montreal, Montreal, Canada. E-mails: cristobal.ochoa.luna@mail.mcgill.ca, philippe.archambault@mcgill.ca*
§*Mechanical Engineering Department, University of Wisconsin-Milwaukee, WI, USA. E-mail: rahmanmh@uwm.edu*

(Accepted July 18, 2018. First published online: August 8, 2018)

SUMMARY
This paper investigates the passive and active control strategies to provide a physical assistance and rehabilitation by a 7-DOF exoskeleton robot with nonlinear uncertain dynamics and unknown bounded external disturbances due to the robot user's physiological characteristics. An Integral backstepping controller incorporated with Time Delay Estimation (BITDE) is used, which permits the exoskeleton robot to achieve the desired performance of working under the mentioned uncertainties constraints. Time Delay Estimation (TDE) is employed to estimate the nonlinear uncertain dynamics of the robot and the unknown disturbances. To overcome the limitation of the time delay error inherent of the TDE approach, a recursive algorithm is used to further reduce its effect. The integral action is employed to decrease the impact of the unmodeled dynamics. Besides, the Damped Least Square method is introduced to estimate the desired movement intention of the subject with the objective to provide active rehabilitation. The controller scheme is to ensure that the robot system performs passive and active rehabilitation exercises with a high level of tracking accuracy and robustness, despite the unknown dynamics of the exoskeleton robot and the presence of unknown bounded disturbances. The design, stability, and convergence analysis are formulated and proven based on the Lyapunov–Krasovskii functional theory. Experimental results with healthy subjects, using a virtual environment, show the feasibility, and ease of implementation of the control scheme. Its robustness and flexibility to deal with parameter variations due to the unknown external disturbances are also shown.

KEYWORDS: Backstepping integral control, Time delay estimation, Passive and active rehabilitation, Time delay error

1. Introduction

Neurological diseases have become a challenging problem for the scientific community, as confirmed by the statistics of World Health Organization (WHO). Each year, at least 15 million people worldwide suffer from neurological diseases, such as strokes.[1] Among them, 6 million die and 5 million more are living with a permanent disability.[1] The consequences of a stroke can vary from mild to very severe depending on the nature of the stroke, the injured region of the brain, and the degree of damage.[2] Usually, the stroke survivors do not have the means of performing daily-life activities independently,

* Corresponding author. E-mail: brahim.brahmi.1@ens.etsmtl.ca

https://doi.org/10.1017/S0263574718000723 Published online by Cambridge University Press

such as eating or dressing, due to permanent disability, frequently on one side of the body.[2] This weakness can generate various physical and psychological problems for the stroke victims.

Rehabilitation programs have proven clinically effective. This treatment is able to support people with stroke to recover their inadequate functional capacity, benefit from the acquisition of new skills, and improve their quality of life. However, these programs need intensive and heavy effort by the therapist.[3] New devices such as exoskeleton robots, help overcome the limitations of conventional physiotherapy, attracting much attention from the scientific community.[3] The main benefit of the rehabilitation robots is their ability to provide intensive physiotherapy for the required periods. Another important point is that these robots provide numerous data that allow the physiotherapist to accurately assess the subject's performance.[3] However, a major aspect is that the design of this kind of robot must be harmonious with the human anatomy biomechanics. For this reason and to provide a modern rehabilitation treatment for the upper limb, we have developed an exoskeleton robot named ETS-MARSE (*Motion Assistive Robotic-Exoskeleton for Superior Extremity*).[4–7] This robot is compatible with the human arm configuration and can perform various rehabilitation movements and assistive tasks. All the originality of the designed robot is summarized in refs. [6 and 7].

One of the main goals of the control system applied to these robots is to make the exoskeleton robot perform the human-like motion. However, these robots are characterized by highly nonlinear dynamics due to their complicated mechanical construction and hard nonlinearities[8] (such as nonlinear friction forces, backlash, etc.). Furthermore, the synergy between the human and the exoskeleton makes the robot subject to external and unknown disturbances due to different physiological conditions of the subjects. These conditions include nonlinear biomechanical characteristics of the musculoskeletal system, the varying weights of the upper-limb for each subject, the presence of spasticity in neurological subjects, etc.[8] During a rehabilitation session, the uncertain nonlinear dynamic model and the external disturbances can turn into an unknown function that can deteriorate the robot's performance.[4,5] In such a case, we need to design a robust controller that provides the system with more flexibility and robustness to deal with these problematic characteristics.

Numerous nonlinear control systems have been designed to overcome the effect of the uncertain nonlinear dynamics and unexpected external disturbances, which influence the robot performance, e.g., conventional adaptive control,[9] H_∞ control,[10] and sliding mode control (SMC).[9,11,12] Actually, SMC is considered one of the most robust nonlinear controllers developed to control uncertain dynamics. This control is fundamentally based on a larger high-gain switching controller that pushes the system trajectory to converge to the selected sliding surface.[12] Nevertheless, the high-activity switching gain causes a "chattering" problem[13] that can damage the actuators of the robot. Another successful nonlinear technique, which has been used to control a robot system with a complex dynamic model, is backstepping control.[9,11,14] Backstepping control is characterized by a recursive Lyapunov scheme and a virtual control input, which ensures the stability of the control system. Despite the highly accurate trajectory tracking provided by this approach, backstepping control is very sensitive to the uncertain dynamics and unknown external disturbances.[9,11] Various strategies have been combined with backstepping to improve its robustness against the effect of the nonlinear uncertain dynamics and external disturbances. For example, a conventional adaptive backstepping control was developed in ref. [15], assuming that the dynamic model of the manipulator is linear in a set of physical parameters. However, the hard nonlinearities of the manipulator's dynamic model make the system sensitive to even small disturbances. To overcome this problem, numerous approaches combine backstepping control with fuzzy logic, neural networks, or both.[16–19] However, these strategies need heavy computations that make the implementation very complex. Time delay estimation (TDE) approach may be considered to compensate the uncertainties.[20–22] The TDE has been implemented in many robotic systems with consistently good performance.[20,23–25] TDE utilizes the previous response of the robot system and the previous control input to provide new control actions. However, due to noisy measurements and nonlinearity of signals along the sampling time, a time delay error (TDR) exists, which would deteriorate the robustness and the accuracy of the robot. To the best of our knowledge, no one has proposed a methodic solution to eliminate the influence of this error.

In order to address the mentioned problems, a solution is proposed in this paper by combining a nonlinear integral backstepping control (BI)[26,27] and a TDE to estimate the hard nonlinearity of the system introduced by the uncertain nonlinear dynamics and unknown disturbances. TDR is taken into consideration by estimating its value with a recursive estimator. This latter is an intensive or

https://doi.org/10.1017/S0263574718000723 Published online by Cambridge University Press

repeating action used to turn down the influence of this error on the accuracy of the estimation. The integral control provides a progressive change to reduce the unmodeled error and improve the robustness of the proposed control against the dynamic uncertainties. The structure of the designed nonlinear Backstepping Integral control based on Time Delay Control (BITDC) aims to provide a high-level of robustness and accuracy without any sensitivity to uncertain nonlinear dynamics and unexpected disturbances. This will make the exoskeleton robot perform a smooth movement, similar to the natural human movement, and will supply the control system more flexibility to handle the uncertainties and parameters' variation. The stability of the robot system and the convergence of its errors are formulated and demonstrated based on Lyapunov–Krasovskii functional theory. Moreover, the proposed strategy is characterized as an easy implementation. The efficiency and the robustness of the proposed approach are validated with Cartesian trajectory tracking corresponding to passive physical therapy tasks.

The proposed strategy is not limited to perform the passive rehabilitation but also qualified to perform the active rehabilitation. To complete this protocol, we necessarily rely on the estimation of the desired movement intention (DMI) of the subject using indirect force control. This latter is done by Damped Least Square method (DLS), which has been successfully used in multiple applications.[28−30] The DLS approach aims to provide a compromise between robustness of the solution and accuracy of the robot's performance. Besides, the proposed control is evaluated with healthy subjects using the virtual environment as an interface.[31] This latter is a highly attractive tool, contributing numerous benefits. It authorized the creation of immersive and interactive scenes, where the oriented task can be introduced in the form of earnest games.[32] This interface also helps in stimulation of the subjects and visualizes the performed tasks. This interface permits us to record the performance data of the patient to evaluate accurately his improvement and benefit from its flexibility to adjust the designed functional movement to the requirement of the patient.[32] The comparative study with the conventional approach shows the accuracy, robustness, and flexibility of the proposed controller to deal with unknown dynamics, external disturbances, and parameters variations.

The outline of the paper is organized as follows. The kinematics and dynamics of the robot are presented in the next section. The control scheme is described in section III. Experimental and comparison results are shown in Section IV. Finally, the conclusion is presented in Section V.

2. Description of Kinematics and Dynamics of ETS-MARSE Robot

2.1. Exoskeleton robot development

The developed exoskeleton robot ETS-MARSE is a redundant robot consisting of 7-DOFs, as shown in Fig. 1. It was created to provide physical therapy and assisted motion to the injured upper limb. The idea of the designed exoskeleton is basically extracted from the anatomy of the upper limb of the human, to be ergonomic for the user along with the physical therapy session. The shoulder part consists of three joints; the elbow part comprises one joint, and the wrist part consists of three joints. Each part is responsible for performing a variety of upper-limb motions, as shown in Table II. The design of the ETS-MARSE has special features compared with the existing exoskeleton robots. Among them, it has a comparatively low weight, an excellent power/weight ratio, can be easily fitted or removed, and is capable of adequately compensating for gravity. A new power carrying mechanism was included for supporting the shoulder joint internal/external rotation and for forearm pronation/supination. This robot can be used with a wide range of subjects, due to the length of its adjustable links. This exoskeleton can perform passive (completely support and perform the motion on the subjects' upper limb) and active assistive motion (respond to force, electromyography, and /or be compliant with the subject to accompany and assist him/her in the intended motion). All special characteristics and contribution features of the ETS-MARSE and comparison with similar existing exoskeleton robots are summarized in refs. [6, 7, 33 and 34].

2.2. Kinematics of ETS-MARSE robot

The transformation from Cartesian space to joint space is done by a nonlinear function named the Jacobian matrix ($J(\theta) \in R^{6\times7}$), which links the end-effector Cartesian velocities to the joints angular velocity vector ($\dot{x}_d = J(\theta)\dot{\theta}$).[35,36] In order to maneuver the exoskeleton in Cartesian space, we used the inverse Jacobian matrix method, since the proposed control is executed in the joint space. Due

https://doi.org/10.1017/S0263574718000723 Published online by Cambridge University Press

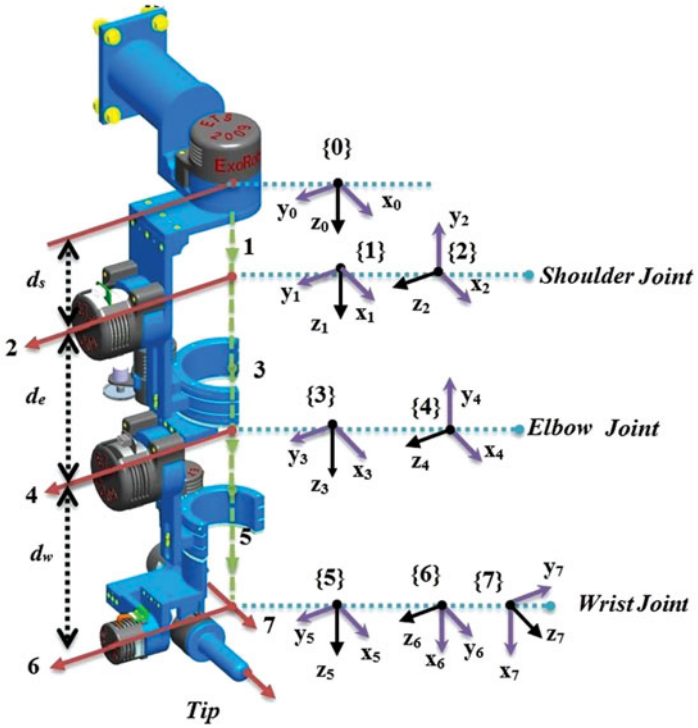


Fig. 1. Reference frames of ETS-MARSE.

to the redundant nature of the ETS-MARSE robot where its Jacobian matrix is not quadratic, the inverse kinematics can be solved using the pseudo-inverse of the Jacobian, which can be expressed as follows:[36]

$$\begin{cases} \ddot{\theta}_d = J^{+}\ddot{x}_d - J^{+}\dot{J}J^{+}\dot{x}_d \\ \dot{\theta}_d = J^{+}\dot{x}_d \end{cases} \tag{1}$$

where $x_d \in R^{6\times 1}$ is the desired Cartesian position and orientation vector of the end-effector, and $\ddot{x}_d,\ \dot{x}_d \in R^{6\times 1}$ are the Cartesian desired acceleration and velocity vectors, respectively. $\ddot{\theta}_d, \dot{\theta}_d \in R^{7\times 1}$ are the calculated joint acceleration and velocity respectively, and $J^{+} = J^{T}(JJ^{T})^{-1}$ is pseudo-inverse generalized.[36] The proposed joint-space based control in this paper does not need a Jacobian matrix or inversion of a Jacobian matrix, as for a Cartesian space-based controller. The role of the Jacobian matrix and its inverse here is the generation of the desired rehabilitation trajectory. Hence, the singularity is not an issue in this case.[34] Moreover, the singularities of the exoskeleton robot are known to us; they will appear when the ETS-MARSE is straight down ($\theta 2 = 0^{\circ}$, and/or $\theta 4 = 0^{\circ}$, and/or $\theta 6 = -90^{\circ}$). As well, a singularity will happen when the axes of rotation of joint-1 (Z1), and joint-3 (Z3), and/or joint-5 (Z5), and/or joint-7 (Z7) are aligned with each other.[34] By knowing these cases, we can easily define the trajectory by avoiding all kinematics singularities. More details about the singularities of ETS-MARSE can be found in ref. [34].

The modified Denavit–Hartenberg (DH)[35] parameters are given in Table I. These parameters are obtained from frames reference as shown in Fig. 1, and are used to obtain the homogeneous transformation matrices.

The workspace of the designed robot is given in Table II. The details of the parameters and design of ETS- MARSE are given in ref. [6].

2.3. Dynamics of ETS-MARSE robot

The dynamics behavior of ETS-MARSE is given by the following expression using the Lagrangian approach:[35]

$$M(\theta)\ddot{\theta} + C\left(\theta, \dot{\theta}\right)\dot{\theta} + G(\theta) + f_{ex} = \tau \tag{2}$$

https://doi.org/10.1017/S0263574718000723 Published online by Cambridge University Press

Table I. Modified Denavit–Hartenberg parameters.

Joint (i)	α_{i-1}	a_{i-1}	d_i	θ_i
1	0	0	d_s	θ_1
2	$-\pi/2$	0	0	θ_2
3	$\pi/2$	0	d_e	θ_3
4	$-\pi/2$	0	0	θ_4
5	$\pi/2$	0	d_w	θ_5
6	$-\pi/2$	0	0	$\theta_6-\pi/2$
7	$-\pi/2$	0	0	θ_7

Table II. Workspace ETS-MARSE.

Joints	Motion	Workspace
1	Shoulder joint horizontal flexion/extension	0°/140°
2	Shoulder joint vertical flexion/extension	140°/0°
3	Shoulder joint internal/external rotation	−85°/75°
4	Elbow joint flexion/extension	120°/0°
5	Forearm joint pronation/supination	−85°/85°
6	Wrist jointUlnar/radial deviation	−30°/20°
7	Wrist joint flexion/extension	−50°/60°

where $\theta, \dot{\theta}$, and $\ddot{\theta} \in R^7$ are, respectively, the joints position, velocity, and acceleration vectors, $M(\theta) \in R^{7\times7}$ is the symmetric, positive definite inertia matrix, $C(\theta, \dot{\theta})\dot{\theta} \in R^7$ is the Coriolis and centrifugal vector, $G(\theta) \in R^7$ is the gravitational vector, $\tau \in R^7$ is the torque vector, $f_{ex} \in R^7$ is the external disturbances vector. Without loss of generality, the matrices of dynamic model (2) can be rewritten as follows:

$$\begin{cases} M(\theta) = M_0(\theta) + \Delta M(\theta) \\ C\left(\theta, \dot{\theta}\right) = C_0\left(\theta, \dot{\theta}\right) + \Delta C\left(\theta, \dot{\theta}\right) \\ G(\theta) = G_0(\theta) + \Delta G(\theta) \end{cases} \tag{3}$$

where $M_0(\theta)$, $C_0(\theta, \dot{\theta})$, and $G_0(\theta)$ are, respectively, the known inertia matrix, the Coriolis/centrifugal matrix and the gravity vector. $\Delta M(\theta)$, $\Delta C(\theta, \dot{\theta})$, and $\Delta G(\theta)$ are the uncertain parts.

Let us introduce a new variable such that: $\eta_1 = \theta$ and $\eta_2 = \dot{\theta}$; hence, the dynamic model expressed in (2) can be rewritten as follows:

$$\begin{cases} \dot{\eta}_1 = \eta_2 \\ \dot{\eta}_2 = U(t) + f(t) + H(t) \end{cases} \tag{4}$$

where, $U(t) = U(\eta_1)$; $H(t) = H(\eta_1, \eta_2, \dot{\eta}_2)$ and $f(t) = f(\eta_1, \eta_2)$ this notation is used for easier handling the control scheme with

- $U(\mathrm{t}) = M_0^{-1}(\theta)\tau(t)$
- $H(\mathrm{t}) = M_0^{-1}(\theta)(-f_{ex} - \Delta M(\theta)\ddot{\theta} - \Delta C(\theta, \dot{\theta})\dot{\theta} - \Delta G(\theta))$, and
- $f(\mathrm{t}) = M_0^{-1}(\theta)(-C_0(\theta, \dot{\theta})\dot{\theta} - G_0(\theta))$.

2.4. Problem formulation

One of the main research objectives on this type of robots is to design a controller able to make the human-exoskeleton system achieve passive/active physical therapy movement. This should be performed without accurate information about the dynamics of the robotic system while ensuring a smooth movement similar to natural human motion. Therefore, the designed control scheme should ensure that the measured joint position η_1 of the exoskeleton robot tracks the desired trajectory η_d. Before presenting the control design methodology, we state the properties and the assumptions used in this paper:

https://doi.org/10.1017/S0263574718000723 Published online by Cambridge University Press

Property (1):[37] The known part of inertia matrix $M_0(\theta)$ is symmetric and positive definite for all $\theta \in R^7$ and satisfying $\gamma_{\min}(M_0(\theta))I_{7\times7} \leq M_0(\theta) \leq \gamma_{\max}(M_0(\theta))I_{7\times7}$, where $\gamma_{\min}$ and $\gamma_{\max}$ are minimum and maximum eigenvalue of known inertia matrix $M_0(\theta)$ and $I_{7\times7}$ is identity definite matrix.

Assumption (1): The joints' positions are measured and the corresponding velocities are found from the filtered positions.

Assumption (2): The function $H(t)$ is globally Lipschitz function.

Assumption (3): The variation of the uncertainties parameters $H(t)$ in time is continuous and bounded with known delay t_d. It can be written as

$$H(t) = H(t - t_d) + \varepsilon(t) \tag{5}$$

where $\varepsilon(t)$ is a vector of the delay error of uncertainties variation and t_d is the sampling time period.

Assumption (4): The desired trajectory is bounded.

Assumption (5): The Jacobian matrix $J(\eta_1)$ is known and nonsingular in a finite workspace.

Assumption (6): The external disturbance f_{ex} is supposed to be continuous, has finite energy, and satisfies $f_{ex} \leq \omega$, with an unknown positive disturbance boundary ω.

3. Control Design

In this section, we seek to design the control that is capable of performing both passive and active rehabilitation movements. Passive rehabilitation mode can be achieved by position control. In such case, the exoskeleton performs a predesigned task. On the other hand, the active assistive motion is achieved by the force exerted by the subject on the tip of the robot (wrist joint) and measured by a force sensor. This force is effective to produce some displacement. In our case, we estimate the desired motion intention of the subject from the measured force using DLS.

3.1. Estimation of the desired motion intention (DMI)

This section provides a summary of the estimation method of the DMI. Let us start with the definition of the desired trajectory in the active assistive motion. In this protocol, the desired trajectory is updated as follows:[38]

$$\eta_d = \eta_1 + \Delta\eta_d \tag{6}$$

where $\eta_1 \in R^7$ is the measured joint position, and $\Delta\eta_d \in R^7$ is the estimated of DMI. If $\Delta\eta_d \to 0$, this means that the exoskeleton's wearer stops exercising forces on the force sensor, making the exoskeleton to decrease its motion and progressively, $\eta_d = \eta_1$, the exoskeleton rests in its most recent position. With this mode, the exoskeleton is permitted to catch the user's DMI, while the adaptive tracking control ensures an accurate compensation of the robot dynamic uncertainties and the unexpected bounded disturbances submitted to the robot. Let us now estimate $\Delta\eta_d$ from the user's force, we can use the following equation:[39]

$$F_m = J(\eta_1)\Delta\eta_d \tag{7}$$

where $F_m \in R^6$ is the measured user's force. To solve the Eq. (7), we used DLS or Levenberg–Marquardt stabilization.[40] This approach was originally employed for avoiding the singularity of inverse kinematics solution.[41,42] Rather than merely obtaining the minimum vector $\Delta\eta_d$ that provides the best solution to Eq. (7), we determine the value of $\Delta\eta_d$ that minimizes the quantity:

$$\min_{\Delta\eta_d} J\Delta\eta_d - F_m{}^2 + \lambda^2\Delta\eta_d{}^2 \tag{8}$$

https://doi.org/10.1017/S0263574718000723 Published online by Cambridge University Press

where $0 < \lambda < 1$ is the damping factor and can be determined to be positive depending upon the accurate estimation specifications. Since the sum of Eq. (8) can be written as

$$\left\| \begin{pmatrix} J \\ \lambda I \end{pmatrix} \Delta\eta_d - \begin{pmatrix} F_m \\ 0 \end{pmatrix} \right\|^2 \tag{9}$$

Consequently, the DLS solution is

$$\Delta\eta_d = J^T \left(JJ^T + \lambda^2 I \right)^{-1} F_m \tag{10}$$

Remark 1: The desired trajectory is the input of the proposed controller that will be detailed in the following subsection. Where, in active mode, the desired trajectory is updated by Eq. (6), while in passive mode, the desired trajectory is predefined by a therapist.

3.2. Control algorithm

This section presents the proposed tracking control based on the Backstepping integral approach that can be expressed as follows:

Step 1: Let us define the position error as follows:

$$e\left(t\right) = \eta_1 - \eta_d \tag{11}$$

where, $\eta_d \in R^7$ and $\eta_1 \in R^7$ are the desired and measured trajectories, respectively. Now, we can choose the regulated errors variables as follows:

$$e_1\left(t\right) = \eta_1 - \eta_d + \Gamma \int_0^t e \, dt \tag{12}$$

$$e_2\left(t\right) = \eta_2 - \xi \tag{13}$$

where $\Gamma \in R^{7\times7}$ is a diagonal positive-definite matrix, and ξ is a virtual control input chosen as follows:

$$\xi\left(t\right) = \dot{\eta}_d - \Gamma e\left(t\right) - k_1 e_1 \tag{14}$$

where $k_1 \in R^{7\times7}$ is a diagonal positive-definite matrix. The derivative of the virtual control input (14) is $\dot{\xi}(t) = \ddot{\eta}_d - k_1\dot{e}_1 - \Gamma\dot{e}(t)$.

The time derivative of Eq. (12) is given by

$$\dot{e}_1\left(t\right) = \eta_2 - \dot{\eta}_d + \Gamma e\left(t\right) \tag{15}$$

Substituting Eq. (13) into Eq. (15), we have

$$\dot{e}_1\left(t\right) = \ e_2\left(t\right) + \xi - \dot{\eta}_d + \Gamma e\left(t\right) \tag{16}$$

Consider the first Lyapunov function candidate as

$$V_1 = \frac{1}{2} e_1^T e_1 \tag{17}$$

Taking the time derivative of V_1 as follows:

$$\dot{V}_1 = e_1^T\left(t\right)\dot{e}_1\left(t\right) = e_1^T\left(t\right)\left(e_2\left(t\right) + \xi - \dot{\eta}_d + \Gamma e\left(t\right)\right) \tag{18}$$

Substituting Eq. (14) into Eq. (18), we obtain

$$\dot{V}_1 = -e_1^T\left(t\right) k_1 e_1\left(t\right) + e_1^T\left(t\right) e_2\left(t\right). \tag{19}$$

https://doi.org/10.1017/S0263574718000723 Published online by Cambridge University Press

The first term of Eq. (19) is negative and the second term will be addressed in the next step.

Step 2: Differentiating Eq. (13) with respect to time yields

$$\dot{e}_2(t) = U(t) + f(t) + H(t) - \dot{\xi} \tag{20}$$

Consider the second Lyapunov function candidate as

$$V_2 = V_1 + \frac{1}{2} e_2^T e_2 \tag{21}$$

The time derivative of V_2 is given by

$$\begin{aligned} \dot{V}_2 &= \dot{V}_1 + e_2^T(t)\,\dot{e}_2(t) \\ &= \dot{V}_1 + e_2^T(t)\left(U(t) + f(t) + H(t) - \dot{\xi}\right) \end{aligned} \tag{22}$$

Consider the control law $U(t)$ that stabilizes the robot system such that

$$U(t) = -k_2 e_2(t) - e_1(t) - f(t) - H(t) + \dot{\xi} \tag{23}$$

Substituting Eq. (23) into Eq. (22), we find

$$\dot{V}_2 \leq -e_1^T(t)\,k_1 e_1(t) - e_2^T(t)\,k_2 e_2(t) \tag{24}$$

Relation (24) ensures the global stability of the system. However, $H(t)$ of relation (23) is uncertain and the control law of relation (23) becomes difficult to compute. To overcome this problem, the TDE approach[20] may be used to estimate the uncertainties of the nonlinear robot dynamics. So, if Assumption (2) is verified, $H(t)$ can be estimated such that

$$\hat{H}(t) \approx H(t - t_d) = \dot{\eta}_2(t - t_d) - f(t - t_d) - U(t - t_d) \tag{25}$$

where, t_d is a very small time delay constant. Practically, the smallest constant that can be achieved in real time is the sampling period. However, due to noisy measurements and nonlinearity of signals along the sampling time, a TDR $\varepsilon(t)$ exists. This TDR would deteriorate the robustness and the accuracy of the robot. Unfortunately, the TDR is not available. In this case, let us apply an iterative estimator to estimate and reduce its effect and give more flexibility to the control system on dealing with parameters variation and unexpected disturbances. The iterative estimator is given in scalar form as

$$\begin{aligned} &\hat{\varepsilon}_i(t) = \hat{\varepsilon}_i(t - t_d) - k_{3i} e_{2i}(t) \\ &\hat{\varepsilon}_i(t) = 0,\ \forall t \in [-t_d, 0],\ i \in \{1 \ldots .., 7\} \end{aligned} \tag{26}$$

where, k_{3i} is a positive constant. The proof of Eq. (26) is given in Appendix 1.

We can now apply a feasible control input able to keep the stability of the system even if the dynamics of the robot is uncertain and the external disturbances exist. The proposed controller is given such that

$$U(t) = -k_2 e_2(t) - e_1(t) + \dot{\xi} - f(t) - \hat{H}(t) - \hat{\varepsilon}(t) \tag{27}$$

with the desired torque

$$\tau(t) = M_0 U(t) \tag{28}$$

https://doi.org/10.1017/S0263574718000723 Published online by Cambridge University Press

Before starting the proof of the stabilization of the system, let us define the estimation error of uncertainties using Assumptions (2) and (3) such that

$$\begin{aligned}\tilde{H}(t) &= H(t) - \hat{H}(t) \\ &= H(t) - H(t - t_d) \\ &= \varepsilon(t)\end{aligned} \tag{29}$$

We can now define the estimation error of TDR $\varepsilon(t)$ as

$$\tilde{\varepsilon}(t) = \hat{\varepsilon}(t) - \varepsilon(t) \tag{30}$$

To guarantee the asymptotic stability of the delayed system in the interval $[0, \infty)$, we propose the following Lyapunov–Krasovskii function

$$V_3(t) = V_2(t) + \begin{cases} \sum_{i=1}^{n} \frac{1}{2k_{3i}} \int_0^t \tilde{\varepsilon}_i^2(s)\, ds, \ t \in [0, t_{d1}) \\ \frac{1}{2k_{31}} \int_{t-t_{d1}}^t \tilde{\varepsilon}_i^2(s)\, ds + \sum_{i=2}^{n} \frac{1}{2k_{3i}} \int_0^t \tilde{\varepsilon}_i^2(s)\, ds\ ; \quad t \in [t_{d1}, t_{d2}) \\ \sum_{i=1}^{n-1} \frac{1}{2k_{3i}} \int_{t-t_{di}}^t \tilde{\varepsilon}_i^2(s)\, ds + \frac{1}{2k_{3n}} \int_0^t \tilde{\varepsilon}_n^2(s)\, ds\ ; \quad t \in \left[t_{dn-1}, t_{dn}\right) \\ \sum_{i=1}^{n} \frac{1}{2k_{3i}} \int_{t-t_{di}}^t \tilde{\varepsilon}_i^2(s)\, ds, \ t \in [t_{dn}, \infty) \end{cases} \tag{31}$$

with

$$V_2(t) = \frac{1}{2} e_1^T(t)\, e_1(t) + \frac{1}{2} e_2^T(t)\, e_2(t) \tag{32}$$

The derivative of the proposed functional Lyapunov–Krasovskii with respect to time is obtained as follows:

$$\dot{V}_3(t) \leq -e_1^T(t)\, k_1 e_1(t) - e_2^T(t)\, k_2 e_2(t) - \frac{1}{2} \sum_{i=1}^{n} k_{3i} e_{2i}^2 \tag{33}$$

It is clear from (33) that $\dot{V}_3(t)$ is negative, where all gains k_1, k_2, k_{3i} are positive. The proof of the stability is detailed in Appendix 2. The structure of the control scheme is shown in Fig. 2.

4. Experimental and Comparative Study

4.1. Experiment setup

Implementation was carried out on the ETS-MARSE system described below. The system consists of three processing units, the first is a PC where the top-level commands are sent to the robot using LabVIEW interface, i.e. the control scheme selection, joint or Cartesian space trajectory, gain adjustments, etc. This PC also receives the data after the robot task is executed to analyze its performance. The other two processing units are part of a National Instruments PXI platform. First, a NI-PXI 8081 controller card with an Intel Core Duo processor; in this card, the main operating system of the robot and the top-level control scheme are executed. In our case, this is the integral backstepping-based controller as well as the estimation based on TDE approach, at a sampling time of 500 μs. The inverse kinematics algorithm also runs inside this control loop. Finally, at input–output level, a NI PXI-7813R remote input–output card with a field programmable gate array (FPGA) executes the low-level control; i.e., a PI current control loop (sampling time of 50 μs) to maintain the current of the motors required by the main controller. Also, in this FPGA, the position feedback via Hall-sensors (joint position), and basic input–output tasks are executed. Force sensor feedback is important to accurately control the movement of the exoskeleton. A high linearity six axis force sensor

https://doi.org/10.1017/S0263574718000723 Published online by Cambridge University Press

Table III. Physical parameters of ETS-MARSE.

Segment (Fig. 1)	Segment length (cm)	Segment weight (kg)	Center of gravity, CG (cm)			Moment of Inertia, I (kg.m^2)		
			CG_x	CG_y	CG_z	I_{xx}	I_{yy}	I_{zz}
Shoulder joint[a]	14.0	3.47	0.007	−13.82	−9.84	0.0232	0.0148	0.013
Upper arm[b]	25.0 ± 8.825	3.737	−1.31	−9.79	19.5	0.0233	0.0128	0.020
Forearm[c]	26.0 ± 4.75	2.066	−2.93	−16.32	5.89	0.0166	0.0100	0.0126
Joints 6 & 7	Point-6 (Fig. 1)	0.790	−0.035	−12.18	4.17	0.0029	0.0019	0.0012
Hand[d]	7.75 ± 4.75	0.795	6.22	0.00	5.00	0.0010	0.0012	0.0003

[a]Point 0 to point 2 (Fig. 1); [b]point 2 to point 4 (Fig. 1); [c]Elbow to wrist (joint six); [d]joint 7 to knuckle. The mass and inertia properties of the ETS-MARSE were estimated from the CAD modeling using Pro/Engineer software.

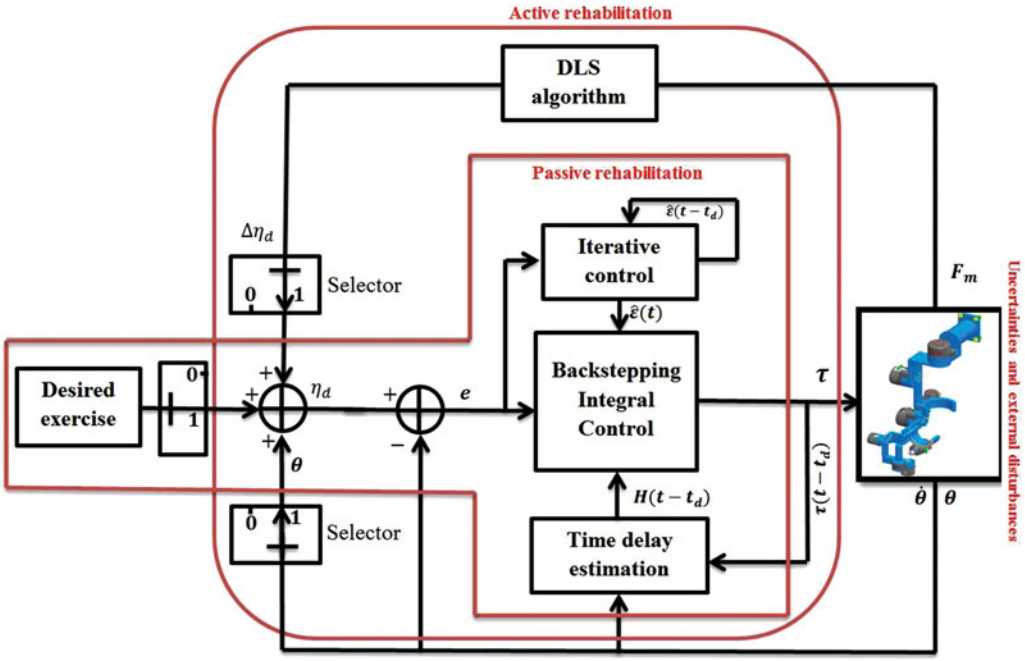


Fig. 2. General schematic of proposed control (for Selector 1 is pass and 0 is stop).

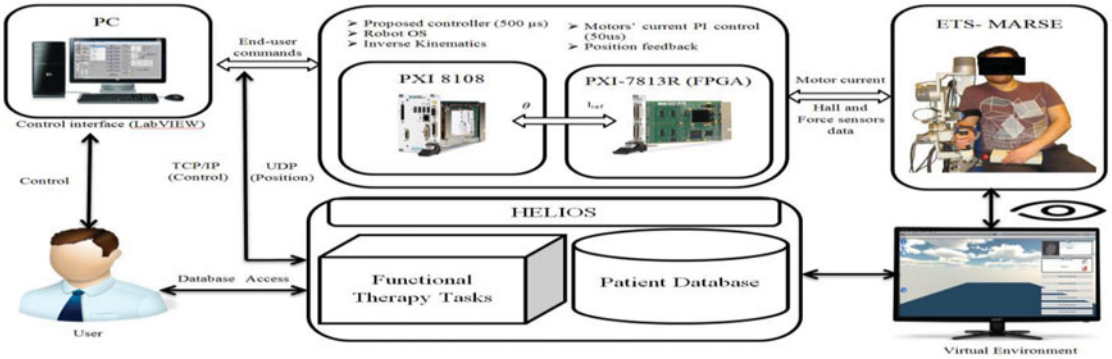
[NANO17-R-1.8-M2-M1PCI, ATI industrial Automation] is so chosen to obtain accurate real-time force measurements. This sensor is mounted on the tip of the robot. The joint of the ETS-MARSE is powered by Brushless DC motors ((Maxon EC-45, EC-90) combined with harmonic drives (gear ratio 120:1 for motor-1, motor-2, and motor-4 and gear ratio 100:1 for motor-3 and motors 5–7).[14,33] The physical parameters of the ETS-MARSE relative to the base reference frame are given in Table III. The diagram of the architecture and overview of the ETS-MARSE system with a human subject is shown in Fig. 3.

The virtual environment HELIOS software was created using the open source "Unity" platform. This interface consists of a set of functional movement tasks defined by a therapist. There are two types of communication with the ETS-MARSE system (LabVIEW). A User Datagram Protocol (UDP) for transferring position data, and a Transmission Control Protocol/Internet Protocol (TCP/IP) for transferring the operator's commands (e.g., start/stop the execution of the task). The choice of these protocols is based on the reliability and the speed of the transmission of data. Our platform contains two profiles: a user profile and an Admin profile. The user profile is under the supervision of a therapist and of a biomedical engineer. This latter is responsible for preparing the rehabilitation session (such as customizing the activities to the patient's needs). The Admin profile is responsible for managing the database of the patient (such Add/Edit/Delete a patient) and has access to the list of all patients and information concerning their rehabilitation sessions.[31]

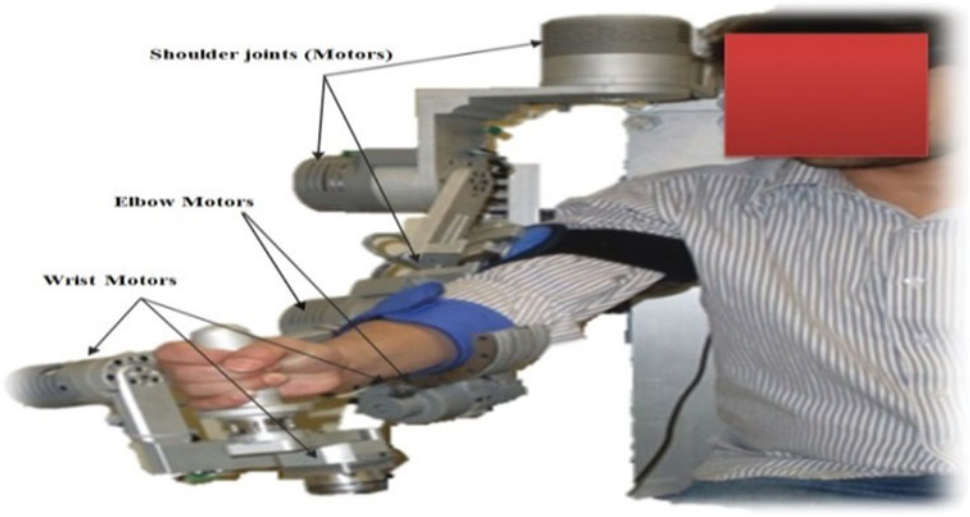
https://doi.org/10.1017/S0263574718000723 Published online by Cambridge University Press

Table IV. Controller parameters.

Gains	Value ($i = 1 : 7$)
k_{1i}	15
k_{2i}	55.5
k_{3i}	0.01
Γ_i	8
λ_i	0.6 ($i = 1$)



(a)

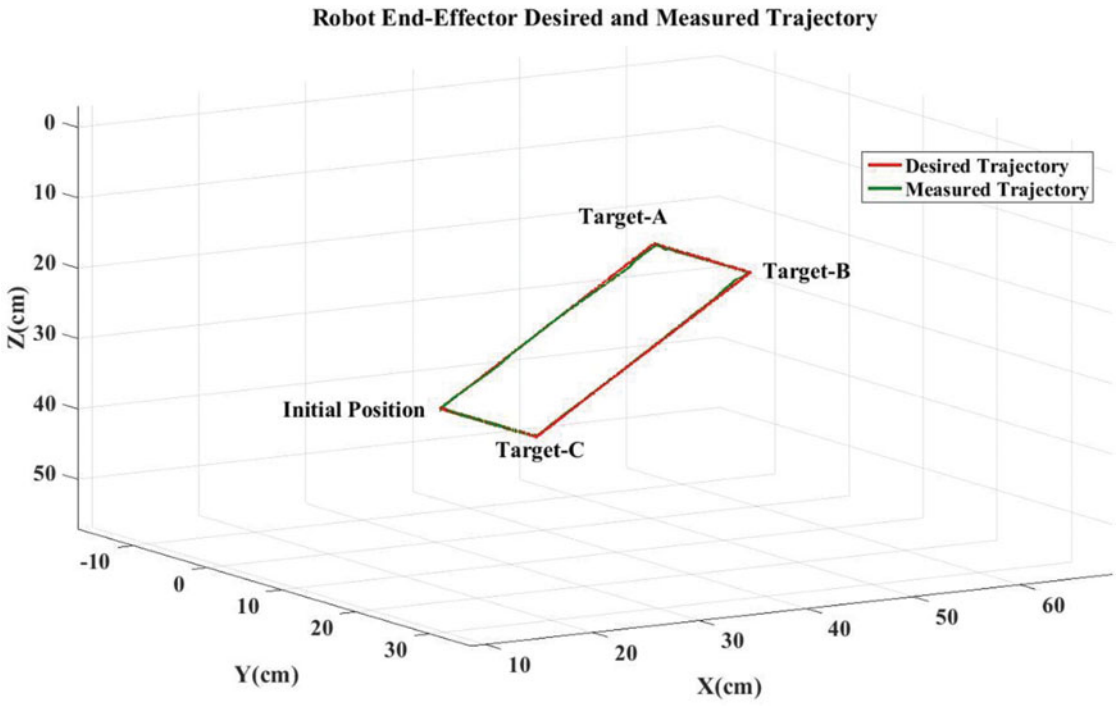


(b)

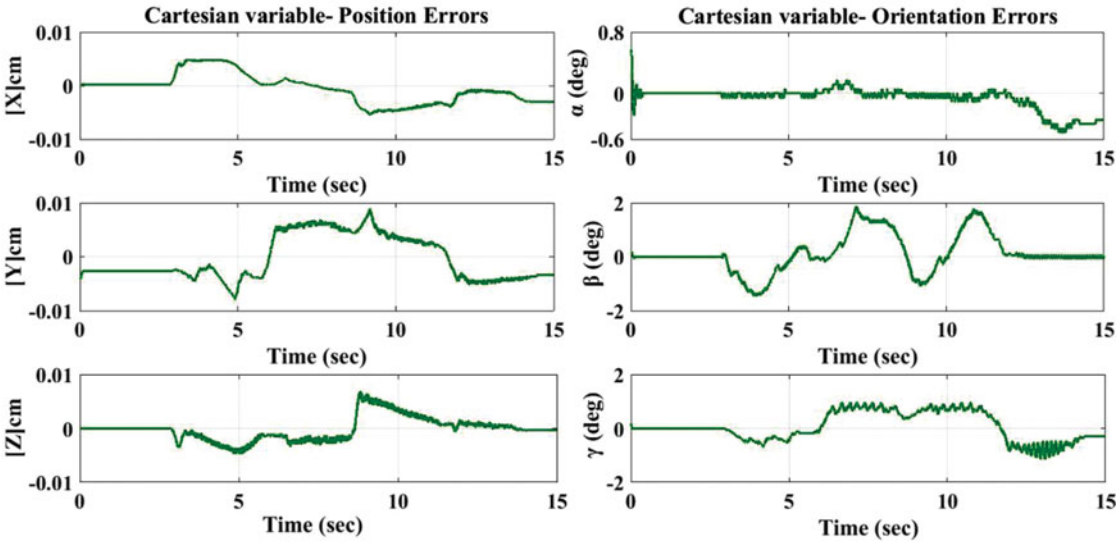
Fig. 3. (A) General schematic of the experimental architecture. (B) Overview of the ETS-MARSE with a human subject.

A rehabilitation session was created to prove the effectiveness of the proposed control system. The physical therapy tasks are performed by three different healthy subjects (average age: 27±4.6 years; average height: 170±8.75 cm; average weight: 75±18 kg). Each subject participated in a full session, under the supervision of a therapist and a control engineer. The role of the therapist is the definition of the range of motion of each subject and the attribution of the suitable exercise. Within the session, the subject was comfortably seated in a chair in front of the virtual interface as we show in Fig. 3(A). The experimental session was divided into two scenarios. In passive rehabilitation, each subject performed the designed task of Fig. 4(A). This task (Initial position→Target-A→Target-B→Target-C→Initial position) is expressed in Cartesian space to evaluate the proposed control. The initial position of the robot is given where elbow joint position is at 90 degrees. This part is followed directly by a

https://doi.org/10.1017/S0263574718000723 Published online by Cambridge University Press



(a)



(b)

Fig. 4. (A) Workspace trajectories of the robot in Cartesian space using the proposed controller, performed by Subject-1: (age: 28 years; height: 177 cm; weight: 83 kg). (B) Cartesian errors.

comparison study with conventional approaches to show the advantage of the proposed controller. In active rehabilitation, each subject has interacted with the virtual environment and tried to track the proposed trajectory. It is important to notice that the external disturbances here are represented by different physiological conditions of the subjects, such as nonlinear biomechanical characteristics of the musculoskeletal system and the different weights of the upper-limb for each subject. The control gains were tuned manually with a trial-and-error approach as shown in Table IV:

https://doi.org/10.1017/S0263574718000723 Published online by Cambridge University Press

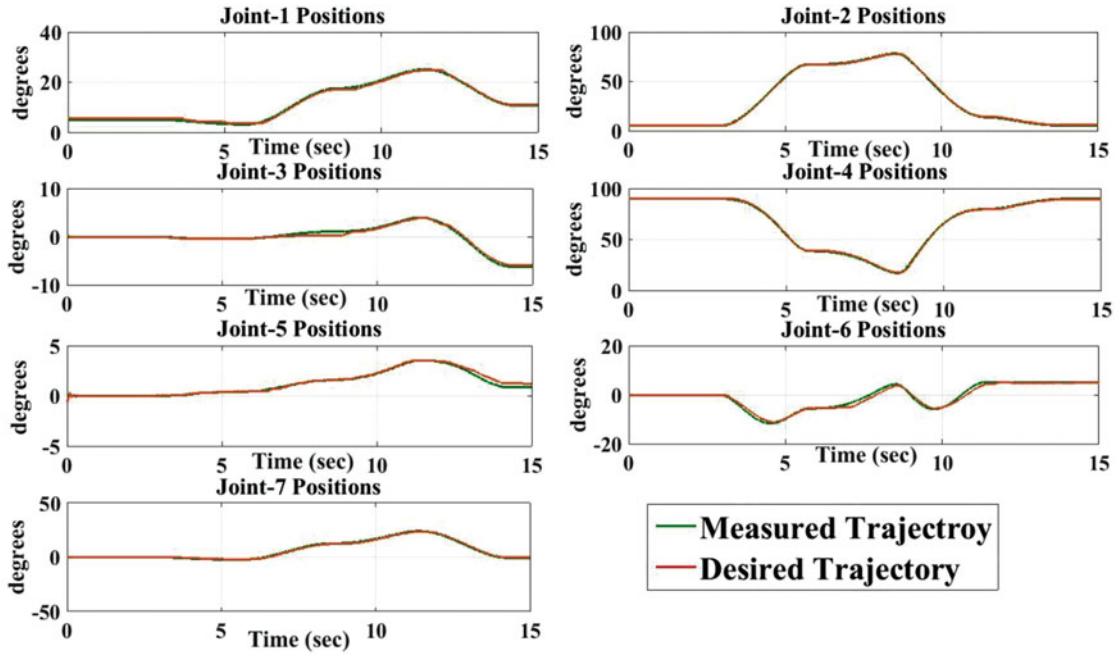


Fig. 5. Position tracking of the robot in joint space corresponding to the movement performed by Subject-1(Fig. 4): (age: 28 years; height: 177 cm; weight: 83 kg).

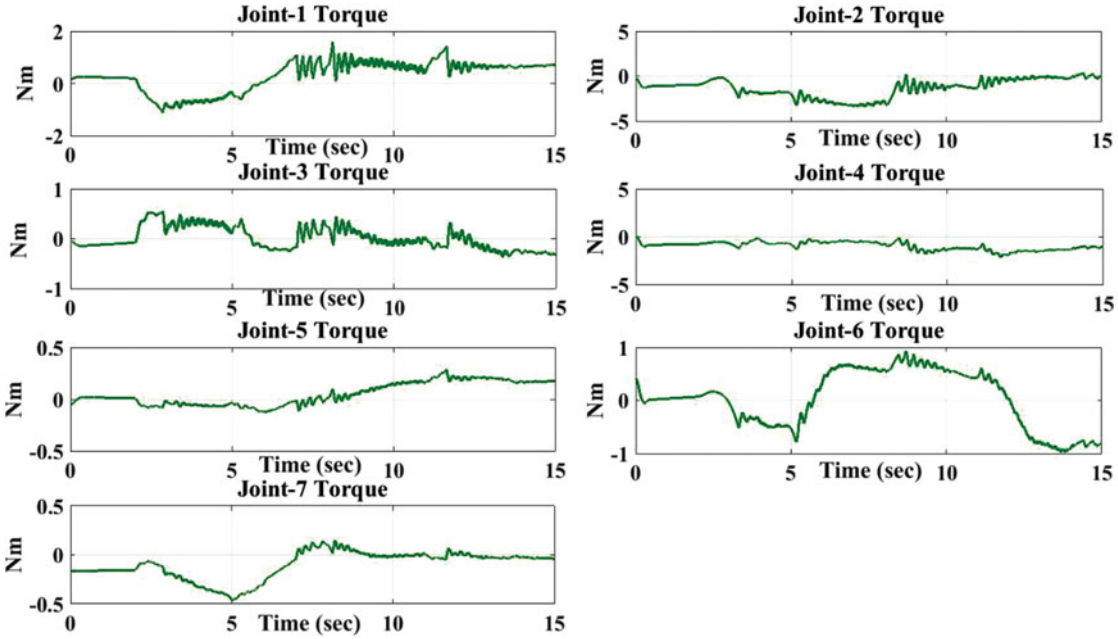


Fig. 6. Control inputs of the proposed controller.

4.2. Experimental results of passive rehabilitation

The experimental results with the ETS-MARSE robot in Cartesian space conducted by Subject-1: (age: 28 years; height: 177 cm; weight: 83 kg) using the proposed control strategy are shown in Figs. 4 and 5. From Figs. 4(A) and 5, we observe that the desired trajectory (red line) nearly overlapped with the measured trajectory (green line). In this case, we can say that these results are reasonably good. Figure 4(B) presents the Cartesian tracking errors as functions of time, where it is clear from this figure that the Cartesian errors are converging and smaller along the desired trajectory. Figure 6 shows that the control input is bounded without any noticeable chattering. So, these results confirm

https://doi.org/10.1017/S0263574718000723 Published online by Cambridge University Press

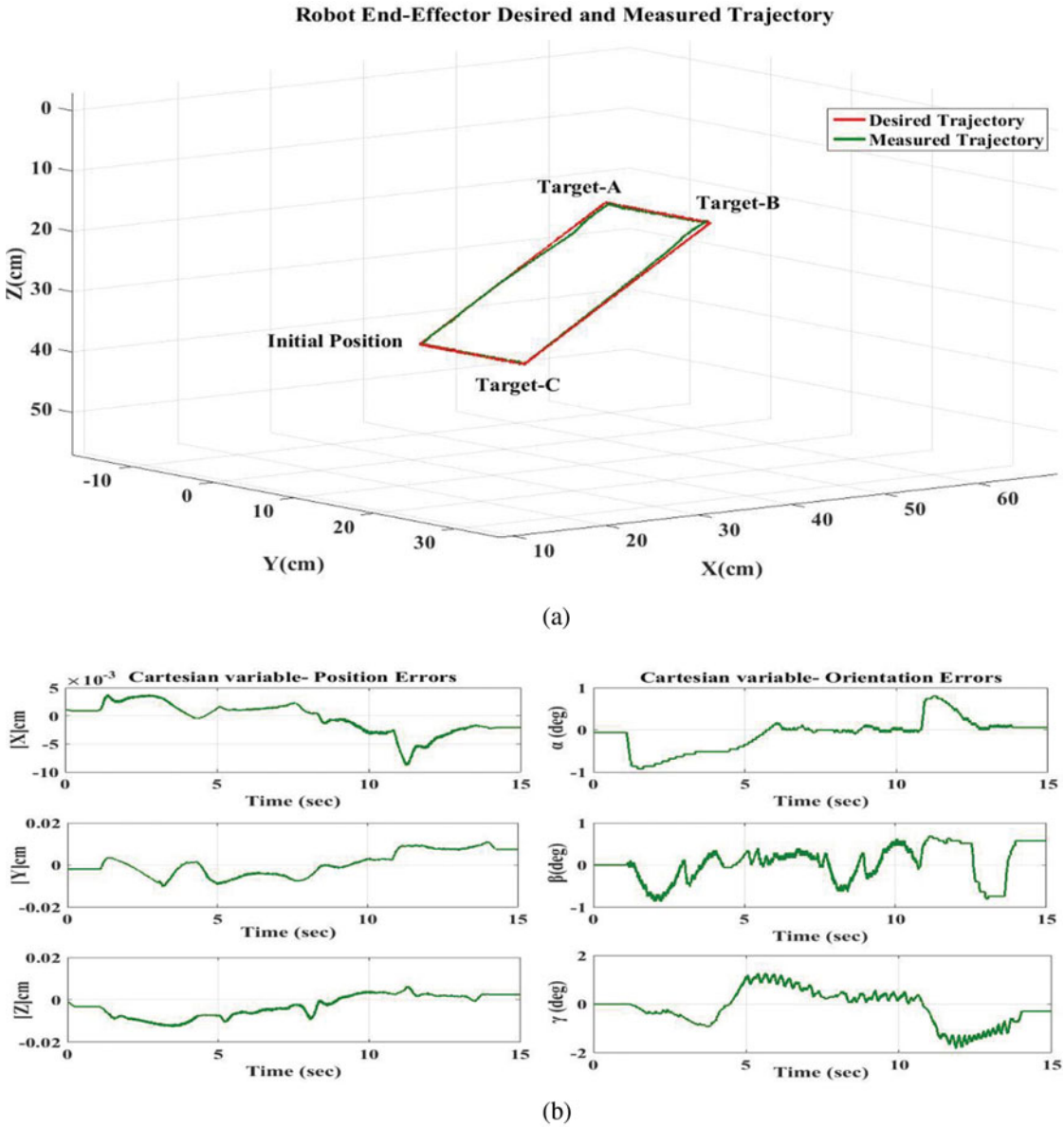


Fig. 7. (A) Workspace tracking of the robot in Cartesian space using the conventional controller, performed by Subject-1: (age: 27 years; height: 177 cm; weight: 83 Kg). (B) Cartesian errors.

that the control strategy is suitable to perform the desired task even when the nonlinear dynamics of the robot are uncertain.

4.3. Comparative study

In order to prove the feasibility and efficiency of the proposed approach, we compared it experimentally with the conventional adaptive tracking control presented in ref. [43]. In this latter, an integral backstepping control combined with TDE has been proposed without considering the effect of TDR. From this comparison, we can see clearly the impact of TDR on the robot's performance and the improvement that is provided by the approach proposed in this paper.

Figures 7(A) and 8 present the Cartesian and joint trajectories tracking (red is the desired trajectory, green is real trajectory) performed by Subject-1: (age: 28 years; height: 177 cm; weight: 83 kg) using the conventional controller. In fact, we remark from figures (Figs. 7(A) and (B) and 8) that the conventional controller shows a good performance. Where, it is certain to ensure that the Cartesian error is getting smaller with time. However, the control inputs of the conventional controller presented

https://doi.org/10.1017/S0263574718000723 Published online by Cambridge University Press

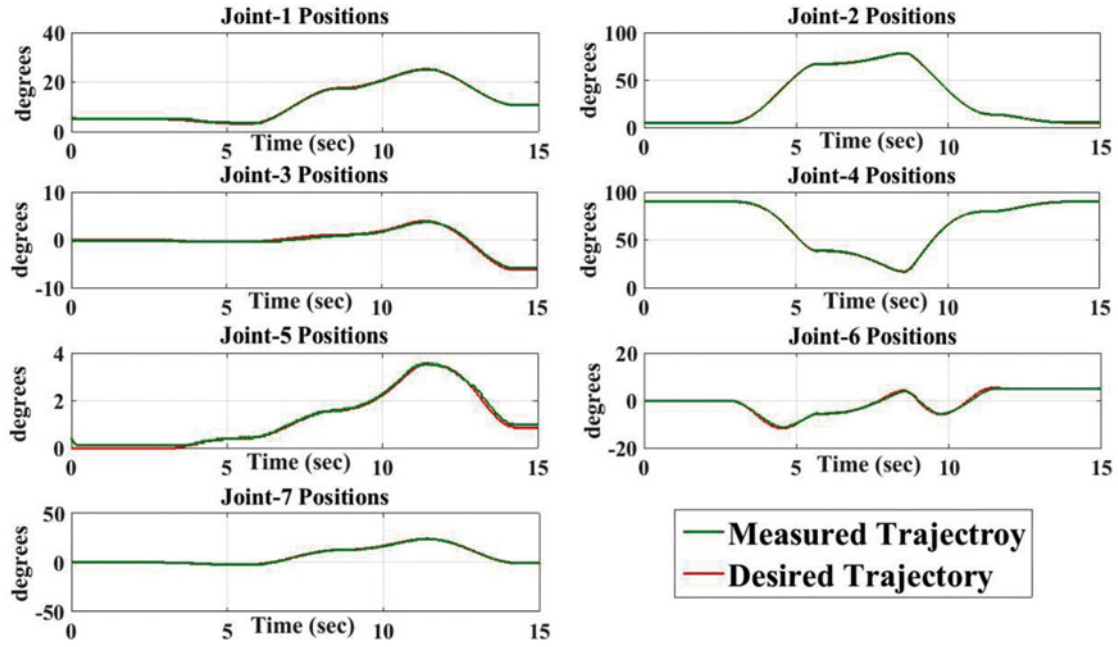


Fig. 8. Position tracking of the robot in joint space corresponding to the movement performed by Subject-1: (age: 28 years; height: 177 cm; weight: 83 kg).

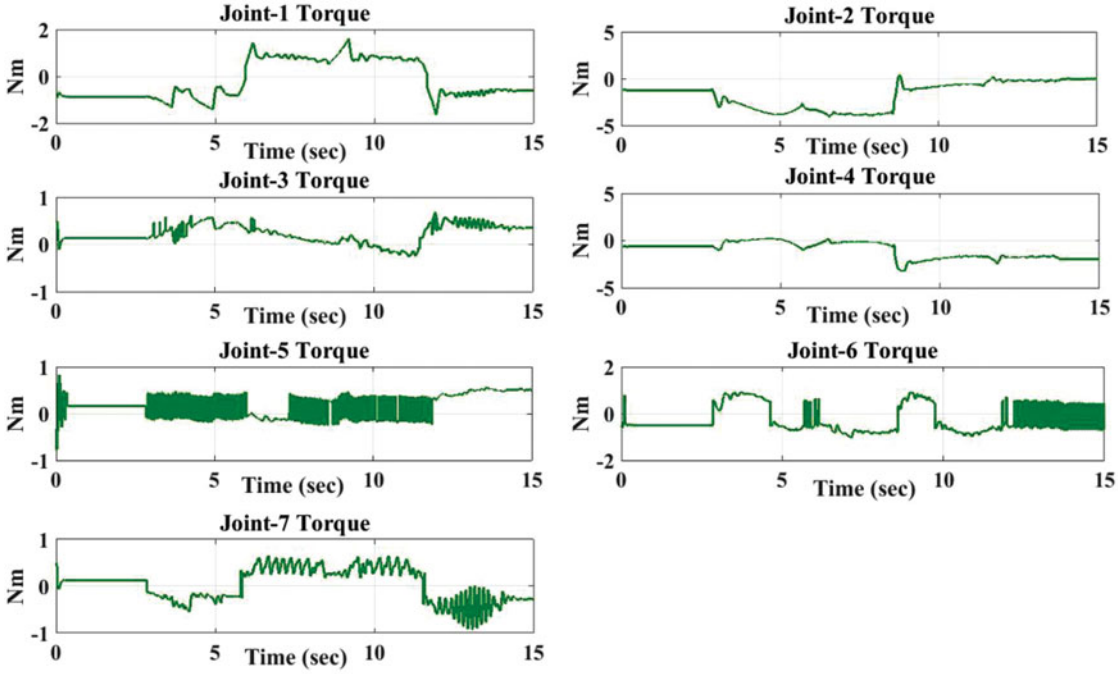


Fig. 9. Control input of the conventional controller.

in Fig. 9 illustrate a noisy signal with chattering phenomenon, while the proposed controller provides a smooth control input (Fig. 6). It is important to remark that we used the same gains' values that employed in the proposed approach. So, the TDR is the main cause of the noise in the control input, which may provoke damage in the motors. From the comparison of the two experimental results, we can conclude that the proposed strategy provides a high level of precision and robustness to the nonlinear uncertain dynamics and unknown disturbances without remarkable chattering, compared with the conventional controller.

https://doi.org/10.1017/S0263574718000723 Published online by Cambridge University Press

Table V. Comparative study.

	Root Mean Square (RMS)			
	Proposed controller		Conventional controller	
Subjects	$\|e\|_{\text{RMS error}}$	$\|\tau\|_{\text{RMS Torque}}$	$\|e\|_{\text{RMS error}}$	$\|\tau\|_{\text{RMS Torque}}$
Subject-1	0.0149	2.9342	0.0408	3.4618
Subject-2	0.0191	2.9061	0.0416	3.4006
Subject-3	0.0165	2.9132	0.0410	4.4994

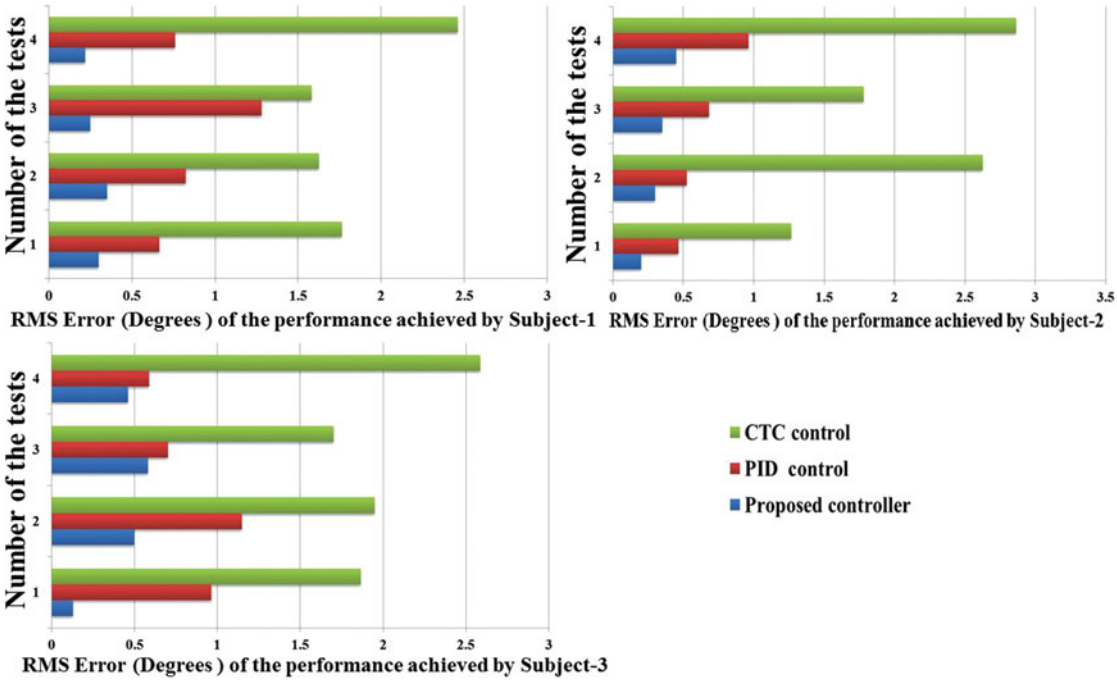


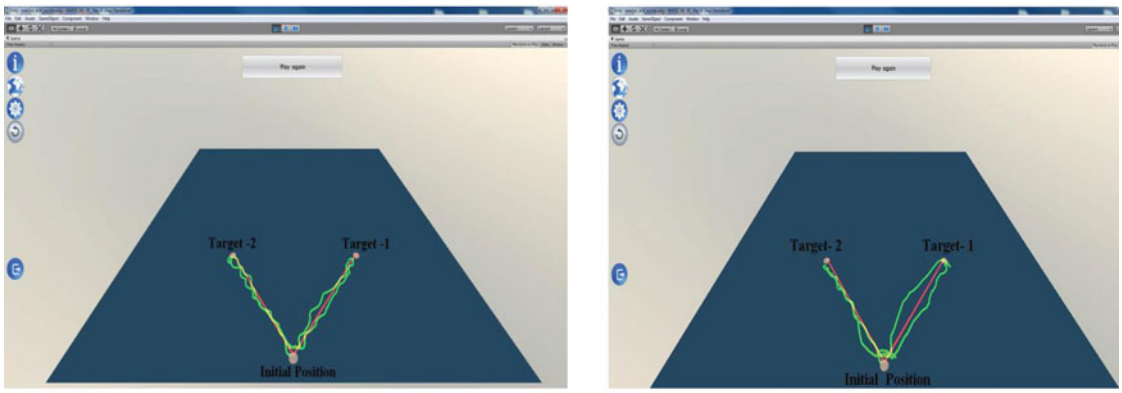
Fig. 10. Comparison performance of the proposed controller with PID controller and CTC controller.

To show more of the feasibility of the designed strategy, we propose a numerical comparison between the above controllers (conventional controller and proposed controller) by calculating the root mean square (RMS) of the error and the control input of each controller as follows: $\|e\|_{\text{RMS}} = \sqrt{\frac{1}{N}\sum_{i=1}^{N}\|e\|^2}$ and $\|\tau\|_{\text{RMS}} = \sqrt{\frac{1}{N}\sum_{i=1}^{N}\|\tau\|^2}$, where N is the number of samples of the signals, corresponding with the time steps of the trial. The evaluation of the controller is given in Table V.

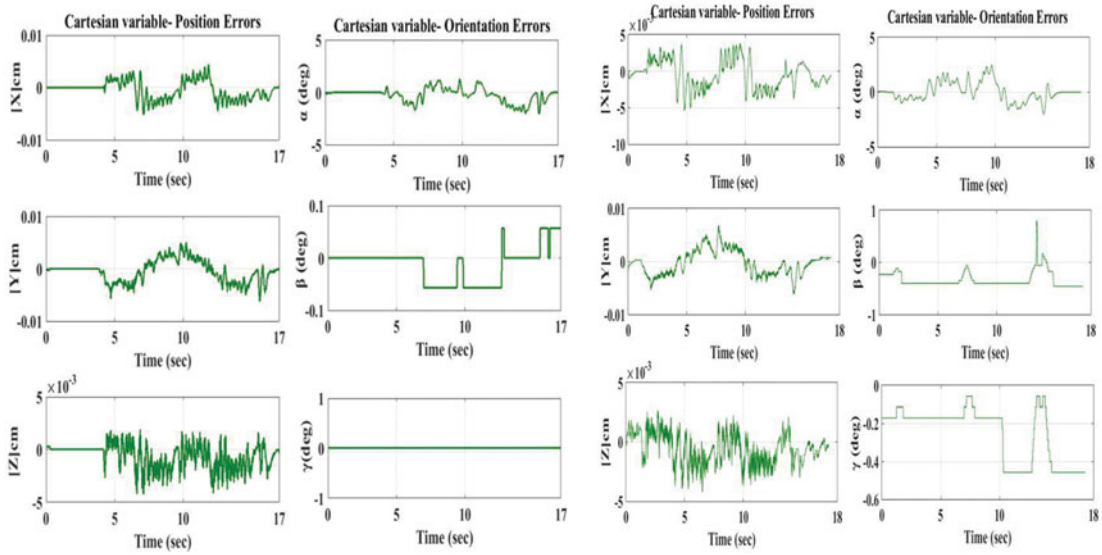
The results in Table V show that the proposed controller gives the robot system a high level of robustness to handle parameter variations, nonlinear uncertainties of the dynamics, and unknown disturbances (the different weight of the upper limb for each subject).

To prove the efficiency of the proposed controller, we provide another comparison study of the proposed controller with classical approaches that are previously applied on the ETS-MARSE robot. The subjects repeated the same tasks using conventional[33](PID controller and Computed Torque Control (CTC)) four consecutive times for each subject, giving a total of 12 experiments for each controller. Figure 10 presents the performance result of each controller with different subjects. It is clear from this figure (Fig. 10) that the proposed control based on TDE presents an excellent performance, much better than PID and CTC and is not affected by parameters' variations. Meanwhile, the PID controller exhibited a more variable behavior, while the CTC controller was the most influenced by variation in the subject's characteristics. The interpretation of these results is that the PID controller fundamentally does not need the dynamic parameters of the exoskeleton robot and its wearer to provide good results. On the other hand, the CTC controller needs these parameters

https://doi.org/10.1017/S0263574718000723 Published online by Cambridge University Press



(a)



(b)

Fig. 11. Workspace tracking of the robot using DLS method performed by Subject-2: (age: 31 years; height: 183 cm; weight: 83.5 kg) (view on Unity platform). (B) Cartesian errors. (A.1). Damping factor λ 6. (A.2). Damping factor λ 45. (B.1). Cartesian error with damping factor λ 6. (B.2). Cartesian error with damping factor λ 45.

to ensure a good performance, so, any variation on these parameters reflects negatively on its performance.

4.4. Experimental results of active rehabilitation

In this section, the subjects tried to follow the proposed triangle task (red line is the desired trajectory and green line is the actual trajectory) under a virtual interface with different values of damping factor λ. In this case, the exoskeleton robot is completely passive and the subject is completely active. The DLS algorithm is used to provide the estimation of the DMI. Figures 11–13 present the results of this experiment.

Figure 11 presents the performance of subject-2 (age: 31 years; height: 183 cm; weight: 83.5 kg) in the virtual interface with help of the ETS-MARSE exoskeleton robot (red line is desired and the green line is the achieved trajectory) using different values of damping factor ($\lambda = 0.6, \lambda = 0.45$). Figures 11–13 present the workspace tracking of the robot in Cartesian space, the control input and the measured force exerted by the subject. It is clear from these plots (Figs. 11–13) that the control strategy achieved the desired performance with small tracking errors and acceptable control input with different values of damping factor. From the good performance of the exoskleton-subject-2 (Fig. 11

https://doi.org/10.1017/S0263574718000723 Published online by Cambridge University Press

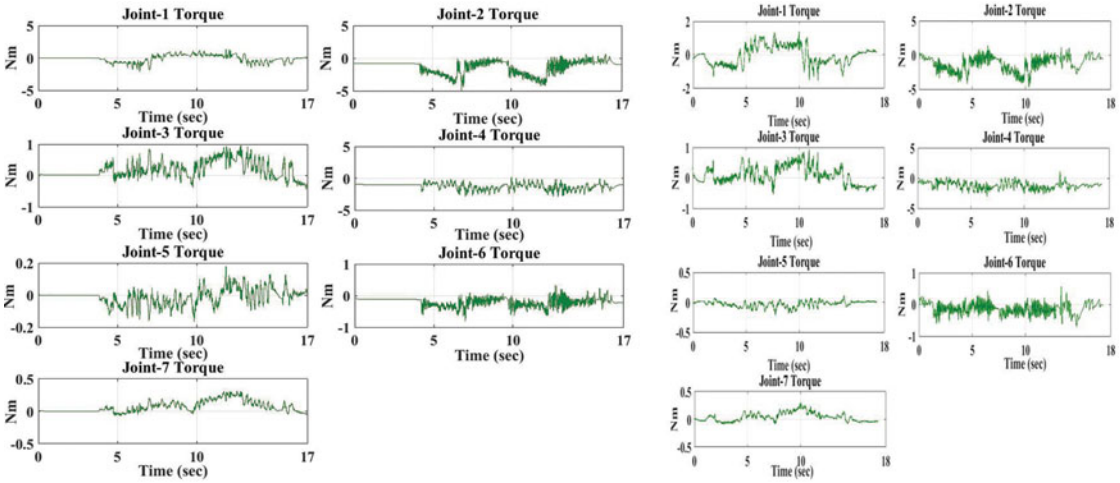


Fig. 12. Torques input of active rehabilitation task. (1). Torque input with damping factor λ 6. (2). Torque input with damping factor λ 45.

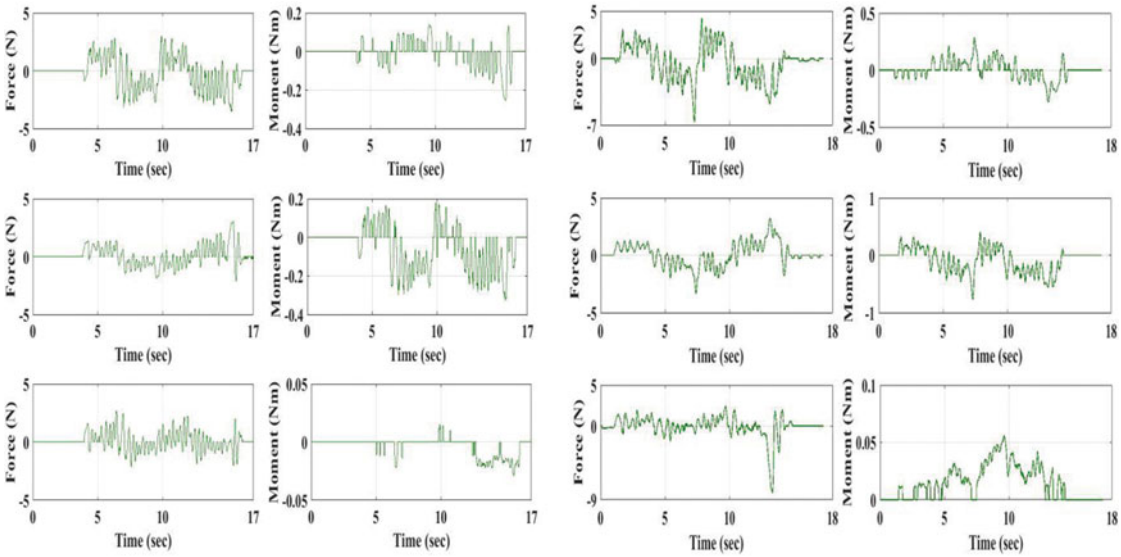


Fig. 13. Measured user's force of the Subject-2: (age: 31 years; height: 183 cm; weight: 83.5 kg). (1). Measured force with damping factor λ 6. (2). Measured force with damping factor λ 45.

with $\lambda = 0.6$), we can infer that the DLS algorithm was qualified to estimate accurately the DMI $\Delta\eta_d$. During the experiment, we concluded that the damping factor λ acts as an influential role to realizing an accurate estimation of the user's intention, as shown in Fig. 11 $\lambda = 0.45$. Despite the controller having ensured a good tracking of the desired user's motion intention, the damping factor affects the estimation accuracy of the desired movement.

5. Conclusion

In this paper, we proposed an adaptive control of an exoskeleton robot with uncertain dynamics based on an integral backstepping controller and TDE. Where, the TDR is taken into consideration. The TDE is used to estimate the robot's nonlinear uncertain dynamics and the unknown bounded perturbations exerted on the exoskeleton robot. To improve the accuracy of the robot performance, the TDR is estimated by a recursive control law to overcome the limitation of TDR inherent of

https://doi.org/10.1017/S0263574718000723 Published online by Cambridge University Press

the TDE approach. The proposed strategy is designed to provide a high-level of robustness and precision to compensate for nonlinear uncertainties of the dynamics and unknown disturbances, to make the exoskeleton robot achieve smooth motion similar to the natural human movement, and to give to the control system more flexibility to deal with the uncertainties and parameters variation. The DLS method has been employed to estimate the DMI of the subjects in order to provide active rehabilitation. The main benefit of the proposed adaptive control approach is that precise knowledge of the dynamic parameters of the robot is not required. Moreover, the proposed adaptive strategy is characterized by the easiness of real-time implementation. The stability analysis of the robot system and the convergence of its errors were proved based on Lyapunov–Krasovskii functional theory. The experimental results prove the effectiveness, facility of implementation, and accuracy of the proposed approach. As a future work, we will seek to overcome the limitations of this approach. In particular, the value of the delayed acceleration for the controller; where the estimation of this variable may deteriorate its accuracy. We are leaning to use this controller with a more complex scenario, such human-robot collaboration.

References

1. S. Sidney, W. D. Rosamond, V. J. Howard and R. V. Luepker, "The 'heart disease and stroke statistics-2013 update' and the need for a national cardiovascular surveillance system," *Circulation* **127**(1), 21–23 (2013).
2. A. De Morand, *Pratique de la Rééducation Neurologique* (Elsevier Masson, Paris, 2014).
3. S. Xie, *Advanced Robotics for Medical Rehabilitation* (Springer, New York, NY, 2016).
4. B. Brahim, S. Maarouf, C. O. Luna, B. Abdelkrim and M. Rahman, "Adaptive Iterative Observer Based on Integral Backstepping Control for Upper Extremity Exoskelton Robot," *Proceedings of the 8th International Conference on Modelling, Identification and Control (ICMIC)*, (2016) pp. 886–891.
5. B. Brahim, M. H. Rahman, M. Saad and C. O. Luna, "Iterative estimator-based nonlinear backstepping control of a robotic exoskeleton world academy of science, engineering and technology," *Int. J. Mech. Aerosp. Ind. Mechatronic Manuf. Eng.* **10**(8), 1313–1319 (2016).
6. M. H. Rahman, M. J. Rahman, O. Cristobal, M. Saad, J.-P. Kenné and P. S. Archambault, "Development of a whole arm wearable robotic exoskeleton for rehabilitation and to assist upper limb movements," *Robotica* **33**(1), 19 (2015).
7. M. H. Rahman, M. Saad, J.-P. Kenné and P. S. Archambault, "Control of an exoskeleton robot arm with sliding mode exponential reaching law," *Int. J. Control, Autom. Syst.* **11**(1), 92–104 (2013).
8. B. Brahim, C. Ochoa-Luna, M. Saad, M. Assad-Uz-Zaman, M. R. Islam and M. H. Rahman, "A New Adaptive Super-Twisting Control for an Exoskeleton Robot with Dynamic Uncertainties," *Proceedings of the 2017 IEEE Great Lakes Biomedical Conference (GLBC)* (2017) pp. 1–1.
9. J.-J. E. Slotine and W. Li, *Applied Nonlinear Control* (Prentice-Hall Englewood, Cliffs, NJ, 1991).
10. G. Rigatos, P. Siano and M. Abbaszadeh, "Nonlinear H-infinity control for 4-DOF underactuated overhead cranes," *Trans. Inst. Meas. Control* **40**(7), 2364–2377 (2017).
11. H. K. Khalil and J. Grizzle, *Nonlinear Systems* (Prentice hall, New Jersey, 1996).
12. K. D. Young, V. I. Utkin and U. Ozguner, "A control engineer's guide to sliding mode control," *IEEE Trans. Control Syst. Technol.* **7**(3), 328–342 (1999).
13. L. Fridman, "The Problem of Chattering: An Averaging Approach," *Variable Structure Systems, Sliding Mode and Nonlinear Control* (Springer, 1999) pp. 363–386.
14. B. Brahmi, M. Saad, M. H. Rahman and C. Ochoa-Luna, "Cartesian trajectory tracking of a 7-DOF exoskeleton robot based on human inverse kinematics," *IEEE Trans. Syst. Man Cybernetics: Syst.* **PP**(99), 1–12 (2017).
15. J. Zhou and C. Wen, *Adaptive Backstepping Control of Uncertain Systems: Nonsmooth Nonlinearities, Interactions or Time-Variations* (Springer-Verlag, Berlin Heidelberg, 2008).
16. W. Chen, S. S. Ge, J. Wu and M. Gong, "Globally stable adaptive backstepping neural network control for uncertain strict-feedback systems with tracking accuracy known a priori," *IEEE Trans. Neural Networks Learning Syst.* **26**(9), 1842–1854 (2015).
17. Z. Li, Z. Huang, W. He and C.-Y. Su, "Adaptive impedance control for an upper limb robotic exoskeleton using biological signals," *IEEE Trans. Ind. Electron.* **64**(2), 1664–1674 (2017).
18. Z. Li, C.-Y. Su, G. Li and H. Su, "Fuzzy approximation-based adaptive backstepping control of an exoskeleton for human upper limbs," *IEEE Trans. Fuzzy Syst.* **23**(3), 555–566 (2015).
19. B. K. Yoo and W. C. Ham, "Adaptive control of robot manipulator using fuzzy compensator," *IEEE Trans. Fuzzy Syst.* **8**(2), 186–199 (2000).
20. K. Youcef-Toumi and O. Ito, "A time delay controller for systems with unknown dynamics," *J. Dyn. Syst. Meas. Control* **112**(1), 133–142 (1990).
21. B. Brahmi, M. Saad, C. O. Luna, P. Archambault and M. Rahman, "Sliding Mode Control of an Exoskeleton Robot Based on Time Delay Estimation," *Proceedings of the International Conference on Virtual Rehabilitation (ICVR)* (2017) pp. 1–2.

https://doi.org/10.1017/S0263574718000723 Published online by Cambridge University Press

22. B. Brahmi, M. Saad, C. Ochoa-Luna and M. H. Rahman, "Adaptive Control of an Exoskeleton Robot with Uncertainties on Kinematics and Dynamics," *Proceedings of the International Conference on Rehabilitation Robotics (ICORR)* (2017) pp. 1369–1374.
23. M. Jin, J. Lee and K. K. Ahn, "Continuous nonsingular terminal sliding-mode control of shape memory alloy actuators using time delay estimation," *IEEE/ASME Trans. Mechatronics* **20**(2), 899–909 (2015).
24. J. Kim, H. Joe, S.-c. Yu, J. S. Lee and M. Kim, "Time-delay controller design for position control of autonomous underwater vehicle under disturbances," *IEEE Trans. Ind. Electron.* **63**(2), 1052–1061 (2016).
25. I. Karafyllis, M. Malisoff, F. Mazenc and P. Pepe, *Recent Results on Nonlinear Delay Control Systems* (Springer, New York, NY, 2016).
26. R. Skjetne and T. I. Fossen, "On Integral Control in Backstepping: Analysis of Different Techniques," *Proceedings of the American Control Conference* (2004) pp. 1899–1904.
27. Y. Tan, J. Chang, H. Tan and J. Hu, "Integral Backstepping Control and Experimental Implementation for Motion System," *Proceedings of the 2000 IEEE International Conference on Control Applications* (2000). pp. 367–372.
28. Y. Luo, Q. Liu, X. Che and L. Li, "Damped least-square method based on chaos anti-control for solving forward displacement of general 6-6-type parallel mechanism," *Int. J. Adv. Robotic Syst.* **10**(4), 186 (2013).
29. C. Liu, C. Song, Q. Lu, Y. Liu, X. Feng and Y. Gao, "Impedance inversion based on L1 norm regularization," *J. Appl. Geophys.* **120**, 7–13 (2015).
30. P.-A. Gauthier, C. Camier, F.-A. Lebel, Y. Pasco, A. Berry, J. Langlois, C. Verron and C. Guastavino, "Experiments of multichannel least-square methods for sound field reproduction inside aircraft mock-up: Objective evaluations," *J. Sound Vib.* **376**, 194–216 (2016).
31. S. Ferrer, C. Ochoa-Luna, M. Rahman, M. Saad and P. Archambault, "HELIOS: The Human Machine Interface for MARSE Robot," *Proceedings of the 6th International Conference on Human System Interaction (HSI)*, (IEEE, 2013) (2013) pp. 117–122.
32. P. L. Weiss, E. Tirosh and D. Fehlings, "Role of virtual reality for cerebral palsy management," *J. Child Neurol.* **29**(8), 1119–1124 (2014).
33. C. O. Luna, M. H. Rahman, M. Saad, P. Archambault and W.-H. Zhu, "Virtual decomposition control of an exoskeleton robot arm," *Robotica* **34**(07), 1587–1609 (2016).
34. M. H. Rahman, T. Kittel-Ouimet, M. Saad, J.-P. Kenné and P. S. Archambault, "Dynamic modeling and evaluation of a robotic exoskeleton for upper-limb rehabilitation," *Int. J. Inform. Acquisition* **8**(01), 83–102 (2011).
35. J. J. Craig, *Introduction to Robotics: Mechanics and Control* (Pearson Prentice Hall Upper Saddle River, 2005).
36. B. Siciliano, L. Sciavicco, L. Villani and G. Oriolo, *Kinematics* (Springer, 2009).
37. M. W. Spong, S. Hutchinson and M. Vidyasagar, *Robot Modeling and Control* (Wiley, New York, 2006).
38. C. Ochoa Luna, M. Habibur Rahman, M. Saad, P. S. Archambault and S. Bruce Ferrer, "Admittance-based upper limb robotic active and active-assistive movements," *Int. J. Adv. Robot. Syst.* **12**(9), 117 (2015).
39. A. M. Khan, D.-w. Yun, M. A. Ali, K. M. Zuhaib, C. Yuan, J. Iqbal, J. Han, K. Shin and C. Han, "Passivity based adaptive control for upper extremity assist exoskeleton," *Int. J. Control Autom. Syst.* **14**(1), 291–300 (2016).
40. C. L. Lawson and R. J. Hanson, *Solving Least Squares Problems* (SIAM, Philadelphia, PA, 1995).
41. C. W. Wampler, "Manipulator inverse kinematic solutions based on vector formulations and damped least-squares methods," *IEEE Trans. Syst. Man Cybern.* **16**(1), 93–101 (1986).
42. Y. Nakamura and H. Hanafusa, "Inverse kinematic solutions with singularity robustness for robot manipulator control," *ASME, Trans. J. Dyn. Syst. Meas. Control* **108**, 163–171 (1986).
43. Y. Kali, M. Saad, K. Benjelloun and M. Benbrahim, "Control of Uncertain Robot Manipulators Using Integral Backstepping and Time Delay Estimation," *Proceedings of the 13th International Conference on Informatics in Control, Automation and Robotics (ICINCO)* (2016) pp. 145–151.

Appendix

1- Proof of the Eq. (26)[4,18]

For very small sampling time period, it is acceptable to assume that the previous TDR equals the current TDR. In this case, considering

$$\begin{cases} \varepsilon_i(t) \in \varepsilon(t) \\ \hat{\varepsilon}_i(t) \in \hat{\varepsilon}(t) \\ \tilde{\varepsilon}_i(t) \in \tilde{\varepsilon}(t) \\ g(t) \in R \end{cases} \tag{34}$$

https://doi.org/10.1017/S0263574718000723 Published online by Cambridge University Press

where $i \in \{1 \ldots .., 7\}$, $g(t) \in R^7$ will be determined later. Now let us propose the following equation:

$$\begin{cases} \varepsilon_i(t) = \varepsilon_i(t - t_d) \\ \tilde{\varepsilon}_i(t) = \varepsilon_i(t) - \hat{\varepsilon}_i(t) \\ \hat{\varepsilon}_i(t) = \hat{\varepsilon}_i(t - t_d) + g(t) \end{cases} \tag{35}$$

Then: $\frac{d}{dt}\int_{t-t_d}^{t} \tilde{\varepsilon}^T(s)\tilde{\varepsilon}(s)ds = -2\tilde{\varepsilon}^T(t)g(t) - g^T(t)g(t)$

Proof: $\frac{d}{dt}\int_{t-t_d}^{t} \tilde{\varepsilon}^T(s)\tilde{\varepsilon}(s)ds$ is $\tilde{\varepsilon}^T(t)\tilde{\varepsilon}(t) - \tilde{\varepsilon}^T(t - t_d)\tilde{\varepsilon}(t - t_d)$. Considering $\hat{\varepsilon}_i(t) = \hat{\varepsilon}_i(t - t_d) + g(t)$

$$\begin{aligned} \tilde{\varepsilon}_i^2(t - t_d) &= [\varepsilon_i(t - t_d) - \hat{\varepsilon}_i(t - t_d)][\varepsilon_i(t - t_d) - \hat{\varepsilon}_i(t - t_d)] \\ &= \left[\varepsilon_i(t) - \hat{\varepsilon}_i(t) + g^T(t)\right]\left[\varepsilon_i(t) - \hat{\varepsilon}_i(t) + g(t)\right] \\ &= \tilde{\varepsilon}_i^2(t) + 2\tilde{\varepsilon}_i(t)g(t) + g^2(t) \end{aligned} \tag{36}$$

Thus, we can obtain

$$\tilde{\varepsilon}_i^2(t) - \tilde{\varepsilon}_i^2(t - t_d) = -2\tilde{\varepsilon}_i(t)g(t) - g^2(t) \tag{37}$$

Let us now define $g(t)$ function as

$$g(t) = -k_{3i}e_{2i}(t) \tag{38}$$

where $e_{2i} \in R^7$. Substituting Eq. (38) in Eq. (37), we obtain

$$\tilde{\varepsilon}_i^2(t) - \tilde{\varepsilon}_i^2(t - t_d) = 2\tilde{\varepsilon}_i(t)k_{3i}e_{2i}(t) - (k_{3i}e_{2i}(t))^2 \tag{39}$$

Multiplying both sides of Eq. (39) by $\frac{1}{2k_{3i}}$ to obtain

$$\frac{1}{2k_{3i}}\tilde{\varepsilon}_i^2(t) - \frac{1}{2k_{3i}}\tilde{\varepsilon}_i^2(t - t_d) = \tilde{\varepsilon}_i(t)e_{2i}(t) - \frac{k_{3i}}{2}e_{2i}^2(t) \tag{40}$$

2- Stability proof of functional Lyapunov–Krasovskii Eq. (33)

The proposed control law Eq. (27) ensures the asymptotic stability of the system. Where $e_1 \to 0$ and $e_2 \to 0$ as $t \to \infty$. The proof is done in three stages. Stage 1 proves the boundedness of $V_3(t)$ in the interval $[0, t_{dn})$. Stage 2 proves the negativeness of $V_3(t)$ in the interval $[t_{dn}, \infty)$. Stage 3 concludes the asymptotical convergence of tracking errors e_1 and e_2.

Stage 1: Boundedness of $V_3(t)$ in the interval $[0, t_{dn})$.

The derivative of Eq. (31) $V_3(t)$ with respect to time for $t \in [0, t_{d1})$ is given by

$$\dot{V}_3(t) = \dot{V}_2(t) + \sum\nolimits_{i=1}^{n} \frac{1}{2k_{3i}}\tilde{\varepsilon}_i^2(t) \tag{41}$$

Differentiating Eq. (32), $\dot{V}_2(t)$ with respect to time is given such that

$$\dot{V}_2(t) = e_1^T(t)k_1\dot{e}_1(t) + e_1^T(t)e_2(t) + e_2^T(t)\dot{e}_2(t) \tag{42}$$

Substituting Eqs. (14), (16) and (20) into Eq. (42) and applying the control law (27) to find

$$\begin{aligned} \dot{V}_2(t) &= -e_1^T(t)k_1e_1(t) + e_1^T(t)e_2(t) + e_2^T(t)\left(-k_2e_2(t) - e_1(t) - \hat{H}(t) + H(t) - \hat{\varepsilon}(t)\right) \\ &= -e_1^T(t)k_1e_1(t) + e_1^T(t)e_2(t) + e_2^T(t)\left(-k_2e_2(t) - e_1(t) + \left(H(x,t) - \hat{H}(x,t)\right) - \hat{\varepsilon}(t)\right) \end{aligned} \tag{43}$$

https://doi.org/10.1017/S0263574718000723 Published online by Cambridge University Press

From Eq. (29) and Eq. (30), we find

$$\dot{V}_2(t) = -e_1^T(t) k_1 e_1(t) - e_2^T(t) k_2 e_2(t) - e_2^T(t) \tilde{\varepsilon}(t) \tag{44}$$

For t $\in [0, t_{d1})$, we have from Eq. (26): $\hat{\varepsilon}(t) = -k_{3i} e_{2i}$, Hence

$$\begin{aligned} \tilde{\varepsilon}_i^2(t) &= (\varepsilon_i(t) - \hat{\varepsilon}_i(t))^2 \\ &= \varepsilon_i^2(t) - 2\varepsilon_i(t)\hat{\varepsilon}_i(t) + \hat{\varepsilon}_i^2(t) \\ &= \varepsilon_i^2(t) - 2\hat{\varepsilon}_i(t)[\tilde{\varepsilon}_i(t) + \hat{\varepsilon}_i(t)] + \hat{\varepsilon}_i^2(t) \\ &= \varepsilon_i^2(t) + 2k_{3i}\tilde{\varepsilon}_i(t) e_{2i} - (k_{3i} e_{2i}(t))^2 \end{aligned} \tag{45}$$

Therefore, substituting Eq. (44) and Eq. (45) in Eq. (41), the Lyapunov function $\dot{V}_3(t)$ is rewritten as follows:

$$\begin{aligned} \dot{V}_3(t) &= -e_1^T(t) k_1 e_1(t) + e_1^T(t) e_2(t) - e_2^T(t) k_2 e_2(t) - e_2^T(t) \tilde{\varepsilon}(t) \\ &\quad + \sum_{i=1}^{n} \frac{1}{2k_{3i}} \varepsilon_i^2(t) + \sum_{i=1}^{n} \tilde{\varepsilon}_i(t) e_{2i} - \sum_{i=1}^{n} \frac{1}{2k_{3i}} (k_{3i} e_{2i})^2 \\ &= -e_1^T k_1 e_1 - e_2^T k_2 e_2 - \sum_{i=1}^{n} \frac{k_{3i}}{2} {e_{2i}}^2 + \sum_{i=1}^{n} \frac{1}{k_{3i}} \varepsilon_i^2(t) \end{aligned} \tag{46}$$

According to *Assumption (2) and (3)* and Eq. (29), $\varepsilon_i(t)$, $i = 1, \ldots, n$ are bounded. This implies $\dot{V}_3(t)$ is bounded. Hence, $\dot{V}_3(t)$ is bounded in time interval $[0, t_{d1})$.

For $t \in [t_{dn-1}, t_{dn})$, conforming to the derivative of $\dot{V}_3(t)$ with respect to time, we obtain

$$\begin{aligned} \dot{V}_3(t) &= -e_1^T k_1 e_1 - e_2^T k_2 e_2 - e_2^T \tilde{\varepsilon}(t) + \frac{1}{2k_{3n}} \tilde{\varepsilon}_n^2(t) + \sum_{i=1}^{n-1} \frac{1}{2k_{3i}} (\tilde{\varepsilon}_i^2(t) - \tilde{\varepsilon}_i^2(t - t_{dn}) \\ &= -e_1^T k_1 e_1 - e_2^T k_2 e_2 - e_2^T \tilde{\varepsilon}(x,t) + \frac{1}{2k_{3n}} \varepsilon_n^2(t) + \tilde{\varepsilon}_n(t) e_{2n} - \frac{1}{2} k_{3n} e_{2n}^2 \\ &\quad + \sum_{i=1}^{n-1} \tilde{\varepsilon}_i(t) e_{2i} - \frac{1}{2} \sum_{i=1}^{n-1} k_{3i} e_{2i}^2 \\ &= -e_1^T k_1 e_1 - e_2^T k_2 e_2 - e_2^T \tilde{\varepsilon}(t) + \frac{1}{2k_{3n}} \varepsilon_n^2(t) + \sum_{i=1}^{n} \tilde{\varepsilon}_i(t) e_{2i} - \frac{1}{2} \sum_{i=1}^{n} k_{3i} e_{2i}^2 \\ &= -e_1^T k_1 e_1 - e_2^T k_2 e_2 - \frac{1}{2} \sum_{i=1}^{n} k_{3i} e_{2i}^2 + \frac{1}{2k_{3n}} \varepsilon_n^2(t) \end{aligned} \tag{47}$$

It is clear from Eq. (47) that $\dot{V}_3(t)$ is bounded for $t \in [t_{dn-1}, t_{dn})$ because $\varepsilon_i(t)$ is bounded. That means $\dot{V}_3(t)$ is bounded in time interval $[t_{dn-1}, t_{dn})$.

Stage 2: The negativeness of $\dot{V}_3(t)$ in the interval $[t_{dn}, \infty)$.

The derivative of $V_3(t)$ with respect to time for $t \in [t_{dn}, \infty)$ is given by

$$\dot{V}_3(t) = -e_1^T k_1 e_1 - e_2^T k_2 e_2 - e_2^T \tilde{\varepsilon}(x,t) + \sum_{i=1}^{n} \frac{1}{2k_{3i}} \left(\tilde{\varepsilon}_i^2(t) - \tilde{\varepsilon}_i^2(t - t_{di}) \right) \tag{48}$$

We have from Eq. (39): $\tilde{\varepsilon}_i^2(x,t) - \tilde{\varepsilon}_i^2(x, t - t_{di}) = 2k_{3i}\tilde{\varepsilon}_i(t) e_{2i} - k_{3i}^2 e_{2i}^2$. So, Eq. (48) can rewrite as follows:

$$\begin{aligned} \dot{V}_3(t) &= -e_1^T k_1 e_1 - e_2^T k_2 e_2 - e_2^T \tilde{\varepsilon}(t) + \sum_{i=1}^{n} \tilde{\varepsilon}_i(t) e_{2i} - \frac{1}{2} \sum_{i=1}^{n} k_{3i} e_{2i}^2 \\ &= -e_1^T k_1 e_1 - e_2^T k_2 e_2 - \frac{1}{2} \sum_{i=1}^{n} k_{3i} e_{2i}^2 \end{aligned} \tag{49}$$

https://doi.org/10.1017/S0263574718000723 Published online by Cambridge University Press

It is clear from Eq. (49) that $\dot{V}_3(t)$ is semi-negative for $t \in [t_{dn}, \infty)$.

Stage 3: Asymptotic convergence

It is clear from Eq. (31) that $V_3(t)$ is positive definite in $e_1(t)$, $e_2(t)$, $\tilde{\varepsilon}(t_d)$. Since $\dot{V}_3(t)$ is semi-negative definite, and $V_3(t)$ is bounded, this implies that $e_1(t)$, $e_2(t)$, $\tilde{\varepsilon}(t_d)$ and $\hat{H}(t)$ are bounded. In this case, we can utilize Barbalat's lemma to complete the stability proof. From Assumption (3) and the boundedness of $e_1(t)$, $e_2(t)$, and from the boundedness of ξ in Eq. (14), and boundedness of $\dot{\theta}$ in Eq. (13), we conclude that $\dot{e}_1$ is bounded in Eq. (14). $\ddot{\theta}$ is bounded from Eq. (2) and $\ddot{\theta}_d$ is bounded (Assumption (4)), this means that $\dot{e}_2(t)$ is bounded. $\dot{e}_1$, $\dot{e}_2$ are bounded imply that $e_1(t), e_2(t)$ are uniformly continuous. According to Barbalat's theorem $e_1(t) \to 0$ and $e_2(t) \to 0$ as $t \to \infty$ and the proof is completed.

https://doi.org/10.1017/S0263574718000723 Published online by Cambridge University Press